(maximize $-\dot{a}$) or outward (maximize $+\dot{a}$) are logarithmic spirals, the reduced flight-time gain in the high-performance regime is more pronounced for the near-circular planetary target orbits, which require an additional velocity increment for a final circularization of the spiral (so that $\boldsymbol{v}_{\text{sailcraft}} \uparrow\uparrow \boldsymbol{v}_{\text{target}}$). For the transfer to the highly eccentric asteroid 1996FG_3 ($e = 0.35$), where such a circularization is not required, the curve bends at higher characteristic accelerations, and the bending is less pronounced.

The results also show that there is a considerable increase of up to 15% in minimal orbit transfer time if model NPR is used. The mean increase is about 10% for Mercury, Venus, Mars, and Vesta and about 5% for 1996FG_3. The results are in accordance with results obtained by Cichan and Melton,[8] where, using a local trajectory optimization method (direct collocation method), an increase of 7.8% in transfer time had been obtained for a simple Earth–Mars transfer ($a_c \doteq 1.5$ mm/s^2, ENC yields 6.8% for this transfer). For a simple Earth–Venus transfer, an increase of even 24% in transfer time (306 days for $a_c \doteq 0.55$ mm/s^2) had been obtained by Cichan and Melton, which suggests, however, that the trajectory is far from the global optimum (ENC yields a minimum transfer time of 267 days for exactly the same problem). The results are also in good accordance with the results obtained by Colasurdo and Casalino[10] for optimal transfers between coplanar circular orbits.

Conclusions

Minimal transfer times for rendezvous missions to inner solar system bodies have been calculated for perfectly and nonperfectly reflecting solar sailcraft, extending, thereby, the currently available data to moderate-performance sailcraft and to very-high-performance sailcraft. Two performance regimes have been found, one for moderate-performance sailcraft and one for high-performance sailcraft, in which the minimum transfer times can be approximated with very simple functions. For nonperfectly reflective solar sailcraft there is a considerable increase of about 10% in the minimal transfer times as compared to perfectly reflective solar sailcraft. The results demonstrate that, for a thorough mission analysis, the nonperfect reflectivity of the solar sail must be considered through an appropriate SRP force model. The simplification that the nonideal reflectivity of the sail can be taken into account by the use of an overall efficiency factor η should only be made for very preliminary mission feasibility analyses.

References

[1]Sauer, C. G., "Optimum Solar-Sail Interplanetary Trajectories," AIAA Paper 76-792, Aug. 1976.

[2]Leipold, M., Seboldt, W., Lingner, S., Borg, E., Herrmann, A., Pabsch, A., Wagner, O., and Brückner, J., "Mercury Sun-Synchronous Polar Orbiter with a Solar Sail," *Acta Astronautica*, Vol. 39, No. 1, 1996, pp. 143–151.

[3]Leipold, M., Pfeiffer, E., Groepper, P., Eiden, M., Seboldt, W., Herbeck, L., and Unkenbold, W., "Solar Sail Technology for Advanced Space Science Missions," International Astronautical Federation, IAF Paper 01-S.6.10, Oct. 2001.

[4]Dachwald, B., "Optimization of Interplanetary Solar Sailcraft Trajectories Using Evolutionary Neurocontrol," *Journal of Guidance, Control, and Dynamics*, Vol. 27, No. 1, 2004, pp. 66–72.

[5]McInnes, C. R., *Solar Sailing. Technology Dynamics and Mission Applications*, Springer-Verlag, London, 1999, pp. 38–40 and 47–51.

[6]Sauer, C. G., "A Comparison of Solar Sail and Ion Drive Trajectories for a Halley's Comet Rendezvous Mission," AIAA Paper 77-104, Sept. 1977.

[7]Forward, R. L., "Grey Solar Sails," *Journal of the Astronautical Sciences*, Vol. 38, No. 2, 1990, pp. 161–185.

[8]Cichan, T., and Melton, R., "Optimal Trajectories for Non-Ideal Solar Sails," American Astronautical Society, AAS Paper 01-471, Aug. 2001.

[9]Wright, J. L., *Space Sailing*, Gordon and Breach, Philadelphia, 1992, pp. 227, 228.

[10]Colasurdo, G., and Casalino, L., "Optimal Control Law for Interplanetary Trajectories with Nonideal Solar Sail," *Journal of Spacecraft and Rockets*, Vol. 40, No. 2, 2003, pp. 260–265.

D. Spencer
Associate Editor

Three-Dimensional Hypersonic Flow Computations over Reentry Capsule Using Energy Relaxation Method

M. M. Patil,* S. Swaminathan,† and R. Kalimuthu*
Vikram Sarabhai Space Center,
Thiruvananthapuram 695 022, India
and
J. C. Mandal‡
Indian Institute of Technology,
Bombay 400 076, India

Nomenclature

Cp	=	coefficient of pressure
D	=	base diameter, m
E	=	total energy, N/m^2
$\bar{\boldsymbol{F}}$	=	flux vector
M	=	Mach number
$\bar{\boldsymbol{N}}$	=	source-term vector
n	=	unit normal
p	=	pressure, N/m^2
R_N	=	nose radius, m
S	=	surface area, m^2/wave speed in Harten–Lax–van Leer contact, m/s
t	=	time, s
$\boldsymbol{U}$	=	conserved variable vector
u	=	x component of velocity, m/s
V	=	velocity, m/s
Vol	=	volume, m^3
v	=	y component of velocity, m/s
w	=	z component of velocity, m/s
α	=	angle of attack, deg
γ	=	specific heat ratio
γ_1	=	specific heat ratio corresponding to
ε	=	internal energy, m^2/s^2
ε_1	=	internal energy governed by the polytropic law, m^2/s^2
ε_2	=	internal energy advected in the flow, m^2/s^2
λ	=	relaxation rate
ρ	=	density, kg/m^3
Φ	=	internal energy function

Subscripts

i, j, k	=	cell index number along x, y, z, respectively
n	=	unit normal component
x	=	x component
y	=	y component
z	=	z component
1	=	parameters corresponding to ε_1

Superscripts

l	=	left state variable
n	=	time level

Received 13 December 2003; revision received 16 March 2004; accepted for publication 23 March 2004. Copyright © 2004 by the American Institute of Aeronautics and Astronautics, Inc. All rights reserved. Copies of this paper may be made for personal or internal use, on condition that the copier pay the $10.00 per-copy fee to the Copyright Clearance Center, Inc., 222 Rosewood Drive, Danvers, MA 01923; include the code 0022-4650/04 $10.00 in correspondence with the CCC.

*Scientist, Kerala State.
†Division Head, Launch Vehicle Design Group, Kerala State.
‡Associate Professor, Department of Aerospace Engineering, Maharashtra State.

r = right state variable
T = transpose

Introduction

THE space capsule during its reentry flight encounters real-gas flows, which are difficult to analyze, as they are governed by the general pressure laws.[1] Numerical analysis of these flows is carried out with different approximations in pressure laws like the equivalent specific heat ratio,[2] etc. The direct modeling of pressure laws introduces a large number of derivatives leading to a nonlinear equation, which is solved numerically. As a result, computation of real-gas flows is very time consuming. Coquel and Perthame[3] introduced the energy relaxation method (ERM) to analyze the real-gas flows, whereby the solvers devised for perfect gases can be used for real gases. In the energy relaxation method, the nonlinear pressure law, is split into linear and nonlinear parts. The internal energy is split into one governed by the linear polytropic pressure law, and the other one is advection energy, which is carried by the flow. So far, the energy relaxation method is used together with Roe[4,5] and kinetic[4] schemes for one and two-dimensional test problems.

In this Note, an attempt is made to apply ERM with Harten–Lax–van Leer contact (HLLC) flux-splitting scheme[6] using finite volume formulation to solve three-dimensional hypersonic flows over a reentry capsule. The fluxes at the interfaces are reconstructed using second-order MUSCL approach with Venkatakrishnan limiters.[7] In all of the calculations, the time integration is carried out with three-stage Runge–Kutta scheme. The analysis is carried out at two flow conditions: one at Mach number 5 and the other at Mach number 10. The results computed are discussed at the end.

Mathematical Description

The inviscid flow of fluid in thermodynamic equilibrium is modeled by Euler equations:

$$\frac{\partial}{\partial t}\iiint_{\text{Vol}} \boldsymbol{U}\,\mathrm{d}\,\text{Vol} + \iint_{S} \bar{\boldsymbol{F}}\,\mathrm{d}S = 0 \tag{1}$$

where

$$\boldsymbol{U} = (\rho, \rho u, \rho v, \rho w, E)^T, \qquad \bar{\boldsymbol{F}} = \begin{pmatrix} \rho V_n \\ (\rho u V_n + p n_x) \\ (\rho v V_n + p n_y) \\ (\rho w V_n + p n_z) \\ [(E+p)V_n] \end{pmatrix}$$

$$E = \rho[\varepsilon + 0.5(u^2 + v^2 + w^2)]$$

This system is supplemented by the equation of state $p = p(\rho, \varepsilon)$. In such a general case, the nonlinearities involved in the pressure law $p(\rho, \varepsilon)$ strongly influence the flow dynamics, and significant difficulties arise over the numerical solution of Euler equations (1). The aim of the energy relaxation theory[3] is to bypass these difficulties while preserving the correct flow dynamics. The main idea is to consider an energy splitting in the form $\varepsilon = \varepsilon_1 + \varepsilon_2$ to relax the nonlinearities in the pressure law.

Here, the internal energy ε_1 is governed by a simple pressure law, typically a polytropic law, while ε_2 stands for the disturbing nonlinearities, which is simply advected by the flow. One seeks a pressure law of polytropic ideal gas and an internal energy $\Phi(\rho, \varepsilon_1)$ so that the initial system (1) and its associated entropy inequality can be recovered in the limit of an infinite relaxation rate λ from the following system:

$$\frac{\partial}{\partial t}\iiint_{\text{Vol}} \boldsymbol{U}_1\,\mathrm{d}\,\text{Vol} + \iint_{S} \bar{\boldsymbol{F}}_1\,\mathrm{d}S = \iiint_{\text{Vol}} \bar{\boldsymbol{N}}\,\mathrm{d}\,\text{Vol} \tag{2}$$

where

$$\boldsymbol{U}_1 = (\rho, \rho u, \rho v, \rho w, E_1, \rho\varepsilon_2)^T, \qquad \bar{\boldsymbol{F}}_1 = \begin{pmatrix} (\rho V_n) \\ (\rho u V_n + p_1 n_x) \\ (\rho v V_n + p_1 n_y) \\ (\rho w V_n + p_1 n_z) \\ [(E_1 + p_1)V_n] \\ (\rho\varepsilon_2 V_n) \end{pmatrix}$$

$$\bar{\boldsymbol{N}} = \begin{pmatrix} 0 \\ 0 \\ 0 \\ 0 \\ \left\{\lambda\rho^{\lambda}\left[\varepsilon_2^{\lambda} - \Phi\left(\rho^{\lambda}, \varepsilon_1^{\lambda}\right)\right]\right\} \\ \left\{-\lambda\rho^{\lambda}\left[\varepsilon_2^{\lambda} - \Phi\left(\rho^{\lambda}, \varepsilon_1^{\lambda}\right)\right]\right\} \end{pmatrix}$$

$$E_1 = \rho\left[\varepsilon_1 + 0.5(u^2 + v^2 + w^2)\right]$$

and $\rho_1 = (\rho, \varepsilon_1) = (\gamma_1 - 1)\rho\varepsilon_1$ with γ_1 being a given constant greater than unity. For a general pressure law this system (2) is a mathematical artifice, but it appears naturally in high-temperature thermodynamics.[3] The original Euler system (1) will thus be recovered from Eq. (2) in the limit $\lambda \to +\infty$, provided that Φ verifies

$$\begin{aligned} \varepsilon &= \varepsilon_1 + \Phi(\rho, \varepsilon_1) \\ p[\rho, \varepsilon_1 + \Phi(\rho, \varepsilon_1)] &= p_1(\rho, \varepsilon_1) \\ &= (\gamma_1 - 1)\rho\varepsilon_1 \end{aligned} \tag{3}$$

because in this limit $\varepsilon_2 = \Phi(\rho, \varepsilon_1)$. The consistency conditions (3) are thus fulfilled for any given choice of γ_1 (with a value of $\gamma_1 > 1$). In addition to the conservation system (1), it is also required to recover the entropy inequality at equilibrium. The required characterization of the admissible γ_1 is given as

$$\gamma_1 > \sup_{\rho,\varepsilon} \Gamma(\rho, \varepsilon) \qquad \text{where} \qquad \Gamma(\rho, \varepsilon) = 1 + (p, \varepsilon)/\rho \tag{4a}$$

$$\gamma_1 > \sup_{\rho,\varepsilon} \gamma(\rho, \varepsilon) \qquad \text{where} \qquad \gamma(\rho, \varepsilon) = (\rho/p)p,\, \rho + (p, \varepsilon)/\rho \tag{4b}$$

The condition (4) can be regarded as a subcharacteristic condition; it means that the sound speed for internal energy ε_1 must be greater than the real sound speed in the fluid, whereas the energy splitting might seem natural and simple.

Numerical Implementation

The vector $\boldsymbol{U}_{i,j,k}^{n+1}$ is obtained from $\boldsymbol{U}_{i,j,k}^{n}$ in following two steps[3]:
1) First step (relaxation): The relaxation states

$$\boldsymbol{U}_{1,i,j,k}^{n} = \begin{bmatrix} \rho_{i,j,k}^{n} \\ \rho_{i,j,k}^{n} u_{i,j,k}^{n} \\ \rho_{i,j,k}^{n} v_{i,j,k}^{n} \\ \rho_{i,j,k}^{n} w_{i,j,k}^{n} \\ E_{1,i,j,k}^{n} \end{bmatrix}$$

and the internal energy $(\rho_{i,j,k}^{n}\ \varepsilon_{2,i,j,k}^{n})$ are obtained from the relaxation procedure by the consistency relation (3), that is,

$$\begin{aligned} (\gamma_1 - 1)\rho_{i,j,k}^{n}\varepsilon_{1,i,j,k}^{n} &= p\left(\rho_{i,j,k}^{n}\varepsilon_{i,j,k}^{n}\right) \\ \rho_{i,j,k}^{n}\varepsilon_{2,i,j,k}^{n} &= \rho_{i,j,k}^{n}\varepsilon_{i,j,k}^{n} - \rho_{i,j,k}^{n}\varepsilon_{1,i,j,k}^{n} \end{aligned}$$

2) Second step (evolution in time): In this step, the Cauchy problem is solved for $t^n \le t < t^{(n+1)}$:

$$\frac{\partial}{\partial t}\iiint_{\text{Vol}} \boldsymbol{U}_1 \,\mathrm{d}\,\text{Vol} + \iint_S \bar{\boldsymbol{F}}_1(\boldsymbol{U}_1)\,\mathrm{d}S = 0 \tag{5}$$

$$\frac{\partial}{\partial t}\iiint_{\text{Vol}} (\rho\varepsilon_2)\,\mathrm{d}\,\text{Vol} + \iint_S (\rho\varepsilon_2 V_n)\,\mathrm{d}S = 0 \tag{6}$$

with the initial datum $[(\boldsymbol{U}^n_{1,i,j,k})^T, \rho^n_{i,j,k}\varepsilon^n_{2,i,j,k}]^T$ using the second-order finite volume scheme. Denoting the $\bar{\boldsymbol{F}}_1$ numerical flux function for the system (5) and $\bar{\boldsymbol{F}}_2$ for Eq. (6), we get $[(\boldsymbol{U}_{1,i,j,k})^T, \rho_{i,j,k}\varepsilon_{2,i,j,k}]^T$ at time $t^{(n+1-)}$. A three-stage Runge–Kutta scheme is used to advance the solution in time form t^n to $t^{(n+1-)}$. At last the vector $\boldsymbol{U}^{n+1}_{i,j,k}$ is computed as

$$\boldsymbol{U}^{n+1}_{i,j,k} = \left\{[\rho, \rho u, \rho v, \rho w, (E_1 + \rho\varepsilon_2)]^{n+1-}_{i,j,k}\right\}^T$$

A scheme is derived following the standard HLLC solver to evolve $\boldsymbol{U}_1$ in time.[6] The higher-order reconstruction of the flow variables is carried out using the MUSCL approach with the Venkatakrishnan limiter.[7] Here, the numerical flux is given by

$$\bar{\boldsymbol{F}}_1\left(\boldsymbol{U}^{n,l}_1, \boldsymbol{U}^{n,r}_1\right) = \begin{cases} \bar{\boldsymbol{F}}_1\left(\boldsymbol{U}^{n,l}_1\right) & \text{if} \quad S^l > 0 \\ \bar{\boldsymbol{F}}_1\left(\boldsymbol{U}^{n,l^*}_1\right) & \text{if} \quad S^l \le 0 < S^m \\ \bar{\boldsymbol{F}}_1\left(\boldsymbol{U}^{n,r^*}_1\right) & \text{if} \quad S^m \le 0 \le S^r \\ \bar{\boldsymbol{F}}_1\left(\boldsymbol{U}^{n,r}_1\right) & \text{if} \quad S^r < 0 \end{cases}$$

To advect the specific energy ε_2, the numerical flux is defined as

$$\bar{\boldsymbol{F}}_2\left(\rho\varepsilon^{n,l}_2, \rho\varepsilon^{n,r}_2\right) = \begin{cases} \bar{\boldsymbol{F}}_2\left(\rho\varepsilon^{n,l}_2\right) & \text{if} \quad S^l > 0 \\ \bar{\boldsymbol{F}}_2\left(\rho\varepsilon^{n,l^*}_2\right) & \text{if} \quad S^l \le 0 < S^m \\ \bar{\boldsymbol{F}}_2\left(\rho\varepsilon^{n,r^*}_2\right) & \text{if} \quad S^m \le 0 < S^r \\ \bar{\boldsymbol{F}}_2\left(\rho\varepsilon^{n,r}_2\right) & \text{if} \quad S^r < 0 \end{cases}$$

where

$$(\rho\varepsilon_2)^{n,l^*} = (\rho\varepsilon_2)^{n,l}\frac{\left(S^l - V^l_n\right)}{(S^l - S^m)}$$

$$(\rho\varepsilon_2)^{n,r^*} = (\rho\varepsilon_2)^{n,r}\frac{\left(S^r - V^r_n\right)}{(S^r - S^m)}$$

The wave speeds S^l, S^m, S^r in the preceding expressions are computed as given in Ref. 6.

Results

Three-dimensional flows over a ballistic reentry module are computed at two different Mach numbers, 5 and 10. The HLLC solver with energy relaxation method is used for air as perfect gas and molecular vibrating gas. The ballistic reentry module is a blunt bicone (Fig. 1) with 20/25-deg cone angles. The total length is 3.19 and base diameter 3.97 times the nose radius respectively. In all of the test cases reported next, a three-dimensional grid of size $101 \times 51 \times 13$ is used. The boundary conditions are applied using dummy cells. At supersonic inflow boundary the flow variables are specified, whereas the flow variables are extrapolated from interior at the outflow boundary. Flow tangency condition is applied at the solid wall. The symmetry plane boundary condition is specified at the angle of attack plane.

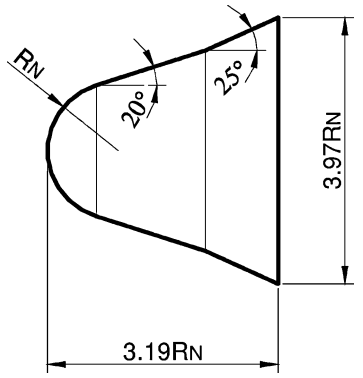

Fig. 1 Reentry capsule.

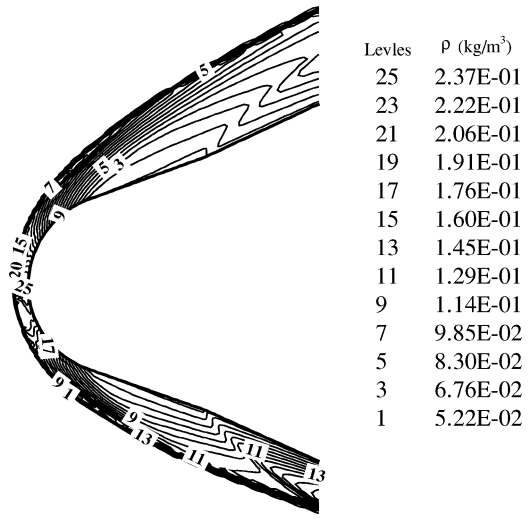

Fig. 2 Computed density contours on reentry capsule at M = 5 and α = 4.66 deg.

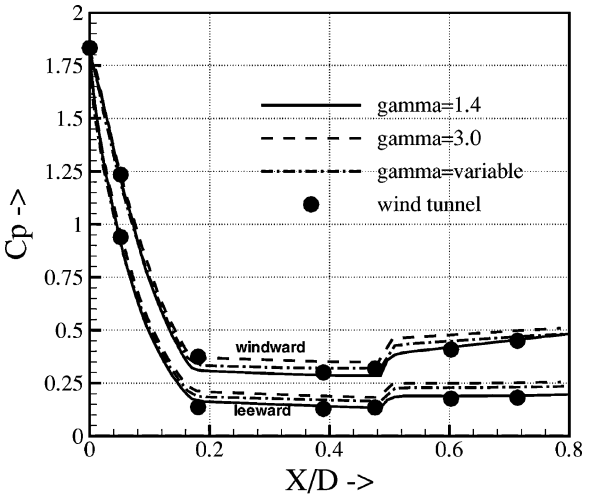

Fig. 3 Surface-pressure distribution on reentry capsule at M = 5 and α = 4.66 deg.

Hypersonic Flow at Mach Number 5

The flow at Mach number 5 and angle of attack 4.66 deg are analyzed, and the computed surface pressure is compared with the wind-tunnel test data.[8] The freestream pressure and temperature are 833 Pa and 63 K, respectively. The angle-of-attack plane of symmetry is assumed for the analysis. Figure 2 shows the computed density contour plot over the reentry module. The flow features like the bow shock as well as the shock at second cone are captured quite well. Figure 3 shows the surface-pressure distribution over the reentry module obtained from the energy relaxation method and

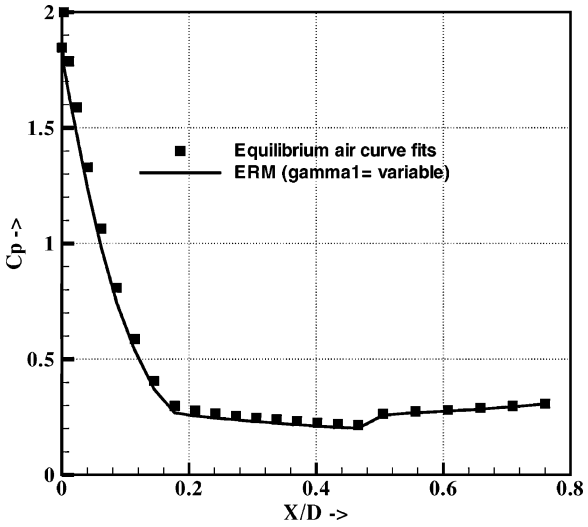

Fig. 4 Surface-pressure distribution on reentry capsule at $M = 10$ and $\alpha = 0$ deg.

wind-tunnel test data.[8] The present solver is used to analyze the flow with energy relaxation method for polytropic index of 1.4, 3, and variable [i.e., the maximum value of the polytropic index is computed at each time step that satisfies the entropy condition (4)]. The computed surface pressure for polytropic index 1.4, that is, with no relaxation of energy compares well with the experimental data in the region of lower temperature. The computed pressure for the higher value of polytropic index compares well in the higher temperature regions, but its value is higher at other regions. This is because, away from the stagnation region, the temperature is lower, where the real-gas effects are less. However, the computed surface pressure is well within the error bands[8] of wind-tunnel test data.

Hypersonic Flow at Mach Number 10

The flow analysis is carried out at the flight condition for Mach number 10 with freestream pressure of 26,500 Pa and density of 0.4122 kg/m^3. This flight condition is generally adopted for the equilibrium code verification and validation. Figure 4 shows the pressure distribution on the body obtained using the energy relaxation method with variable polytropic index and the equilibrium air curve fits. Thus, the energy relaxation method yields quite accurate results.

Conclusions

The energy relaxation method together with HLLC flux splitting has been implemented for three-dimensional real-gas flow analysis over a reentry capsule. The computed pressure compares well with wind-tunnel test data for Mach number 5 and that with air curve-fit data for Mach number 10. From these results, it can be concluded that energy relaxation method together with HLLC flux splitting is an efficient and accurate approach in computing real-gas flows for industrial applications.

Acknowledgments

The authors thank P. Srinivasa for his valuable comments and E. Janardhana for providing encouragement in the work.

References

[1]Vincenti, W., and Kruger, C., *Introduction to Physical Gas Dynamics*, Wiley, New York, 1965, p. 154.

[2]Mottura, L., "An Evaluation of Roe's Scheme Generalized for Equilibrium Real Gas Flows," *Journal of Computational Physics*, Vol. 138, No. 2, 1997, pp. 354–399.

[3]Coquel, F., and Perthame, B., "Relaxation of Energy and Approximate Riemann Solvers for General Pressure Laws in Fluid Dynamics," *SIAM Journal Numerical Analysis*, Vol. 35, No. 6, 1998, pp. 2223–2249.

[4]In, A., "Numerical Evaluation of an Energy Relaxation Method for Inviscid Real Fluids," *SIAM Journal of Scientific Computing*, Vol. 21, No. 1, 1999, pp. 340–365.

[5]Philipe, M., and Shu, C. W., "Real Gas Computation Using an Energy Relaxation Method and High Order WENO Scheme," *Journal of Computational Physics*, Vol. 148, No. 1, 1999, pp. 59–81.

[6]Batten, P., Leschziner, M. A., and Goldberg, U. C., "Average State Jacobians and Implicit Method for Compressible Viscous and Turbulent Flows," *Journal of Computational Physics*, Vol. 137, No. 1, 1997, pp. 38–78.

[7]Venkatakrishnan, V., "On the Accuracy of Limiters and Convergence to Steady State Solutions," AIAA Paper 93-0880, Jan. 1993.

[8]Kalimuthu, R., "Surface Pressure Measurement Results on the SRE (biconic) Configuration at $M = 5$," Vikram Sarabhai Space Center, Internal Rept. VSSC/ATFD/TM_SRE/078/2003, Thiruvananthapuram, India, 2003.

P. Huseman
Associate Editor

Heat Transfer on a Hypersonic Sphere with Diffuse Rarefied-Gas Injection

Vladimir V. Riabov*
Rivier College, Nashua, New Hampshire 03060

Introduction

NUMERICAL and experimental studies[1–3] of aerothermodynamics of hypersonic vehicles have shown that the temperature in the spacecraft nose region can be extremely high, and the maximum value of the heat flux occurs at small values of the nose radius R and small local Knudsen numbers $Kn_{\infty,R}$ that characterize transitional flow regimes from free-molecule medium to continuum.[2–5] Mass injection can be considered as an effective way of the reduction of heat transfer to the surface in this area.[1–6]

The boundary-layer flow with gas blowing was studied by Warren,[6] Libbi and Gresci,[7] and Finley.[8] Only few studies (i.e., Pappas and Lee[9] and Moss[10]) were conducted in the cases of transitional Knudsen numbers. Moss[10] found that mass injection significantly reduces heat transfer to the surface, and when the mass injection rate equals 0.4 of the freestream mass flux the viscous layer is blown completely off the surface, and the heat transfer is zero.

The effect of injecting gaseous coolants on heat transfer in hypersonic perfect gas flow near blunt bodies was studied by Gershbein and Kolesnikov[11] and Emelianova and Pavlov[12] on the basis of the complete system of Navier–Stokes equations and by Moss,[10] Shen et al.,[13] Ankundinov,[14] Provotorov and Stepanov,[15] and Botin[16] on the basis of the thin viscous shock-layer model.[4] Provotorov and Stepanov[15] had found universal relations between the heat flux and the generalized blowing parameters. Heat transfer in the presence of hydrogen blowing and combustion was studied by Riabov and Botin[17] and Botin et al.[18]

These studies have shown that the effectiveness of coolant blowing increases with the decrease of the Knudsen number and becomes significant at $Kn_{\infty,R} < 0.02$. Heat-transfer experimental data[16] received by the method of two-layer thermal-indicator coating[19] confirm this conclusion. Other applications of the gas blowing include the divert and attitude reaction control systems[20] and a counterflow drag-reduction technique in high-speed systems.[21]

Presented as Paper 2004-1176 at the AIAA 42nd Aerospace Sciences Meeting, Reno, NV, 5–8 January 2004; received 17 March 2004; accepted for publication 15 April 2004. Copyright © 2004 by Vladimir V. Riabov. Published by the American Institute of Aeronautics and Astronautics, Inc., with permission. Copies of this paper may be made for personal or internal use, on condition that the copier pay the $10.00 per-copy fee to the Copyright Clearance Center, Inc., 222 Rosewood Drive, Danvers, MA 01923; include the code 0022-4650/04 $10.00 in correspondence with the CCC.

*Associate Professor, Department of Computer Science and Mathematics, 420 S. Main Street. Senior Member AIAA.